

**Poison or Promoter? Investigating the Dual-Role of Carbon Monoxide in
Pincer-Iridium-Based Alkane Dehydrogenation Systems via Operando
Diffuse Reflectance Infrared Fourier Transform Spectroscopy**

Boris Sheludko,^{1,2} Cristina F. Castro,² Alan S. Goldman,¹ Fuat E. Celik^{2*}

¹Department of Chemistry and Chemical Biology

²Department of Chemical and Biochemical Engineering

Rutgers, The State University of New Jersey, Piscataway, NJ

98 Brett Road, Piscataway, New Jersey 08854, United States

* Tel.: +1 848 445 5558. E-mail: fuat.celik@rutgers.edu

Abstract

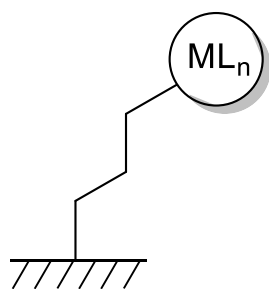
Pincer-ligated iridium complexes of the form $[\text{Ir}(\text{R}^4\text{PCP})\text{L}]$ ($\text{R}^4\text{PCP} = \kappa^3\text{-C}_6\text{H}_3\text{-2,6-}(\text{XPR}_2)_2$; $\text{X} = \text{CH}_2, \text{O}$; $\text{R} = t\text{Bu}, i\text{Pr}$) have previously been shown competent for acceptorless alkane dehydrogenation when supported on silica. It was observed by post-catalysis solid-state NMR that silica-tethered $[\text{Ir}(\text{C}_2\text{H}_4)(\equiv\text{SiO-}^t\text{Bu}_4\text{POCOP})]$ (**3-C₂H₄**) was converted fully to $[\text{Ir}(\text{CO})(\equiv\text{SiO-}^t\text{Bu}_4\text{POCOP})]$ (**3-CO**) at 300 °C. In this work, the characterization of species under dehydrogenation reaction conditions far from equilibrium between butane and butenes (approach to equilibrium $Q/K_{\text{eq}} = 0.3$ at 300 °C) is performed with *operando* Diffuse Reflectance Infrared Fourier-Transform Spectroscopy (DRIFTS) to show the kinetics of species conversion from **3-C₂H₄** to **3-CO**. It is further found that $[\text{IrClH}(\equiv\text{SiO-}^t\text{Bu}_4\text{POCOP})]$ (**3-HCl**), a species considered to be a precatalyst for alkane dehydrogenation, is also fully converted to **3-CO**. A mechanism of decomposition is proposed that implicates surface silanol groups, while carbon monoxide acts as a “stabilizer” for the catalyst by promoting their reductive elimination and maintaining the complex in the I oxidation state.

Key Words

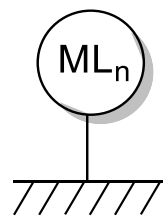
alkane dehydrogenation, pincer ligand, supported molecular catalyst, iridium, DRIFTS, FT-IR

1. Introduction

Catalysts consisting of metal nanoparticles contain many inaccessible bulk atoms. Isolated metal single atom catalysts (SACs) have been explored as promising alternatives due to their increased activity per metal atom.¹⁻⁴ Generally, this terminology has referred to inorganic species consisting of single metal atoms on a supporting material. When thought of in this way, the tunability of SACs relies almost solely on the nature of the support used absent any surface ligands, with many such combinations leading to unstable arrangements ultimately resulting in agglomeration into more stable nanoparticles by mechanisms such as sintering or Ostwald ripening.⁵ The family of SACs also includes individual metal atoms primarily supported by an organic scaffold that often precludes any direct bonds to the support. In this model, the distinction of bonding to the surface at the metal center, as opposed to tethering at a site distal to the metal center, is an important one,⁶ with the latter potentially allowing for the mitigation of deleterious interactions of the metal center with the support, allowing for catalysts to remain more active, or more stable, or both, for longer. Distally tethered complexes are further removed from the surface and, since agglomeration is often a surface-dependent phenomenon, are less likely to form nanoparticles.



Tethered Complex



Metal-Bound Complex

A parallel goal in catalysis has been combining the advantages of homogeneous metal catalysis (primarily inorganic and organometallic complexes) and heterogeneous metal catalysis

(primarily supported nanoparticles).⁷⁻⁸ A common approach, as opposed to generating complexes on the surface of the support used, has been to support or immobilize organometallic complexes on high surface area inorganic supports.⁹⁻²² These strategies frequently work, but only in a narrow range of operating conditions, usually at low temperature, outside of which ligand loss contributes to particle agglomeration and at which point the unique benefits of the ligand field such as enhanced selectivity and active site uniformity are also lost.^{10, 20, 23}

	CHARACTERIZATION	ACTIVITY	SELECTIVITY	HANDLING
HETEROGENEOUS		X		X
HOMOGENEOUS	X		X	
TETHERED	X	X	X	X

One class of complexes that continues to receive attention both as very successful homogeneous as well as, increasingly, heterogenized catalysts, is that of pincer-metal, and particularly pincer-iridium, species of the form $[M(R^4PCP)L_n]$ ($R^4PCP = \kappa^3\text{-C}_6\text{H}_3\text{-2,6-(CH}_2\text{PR}_2)_2$).²⁴ The modularity of these species has made them especially amenable to catalyst development,^{15, 25-27} with multiple derivatives having been synthesized based on the R^4PCP framework,²⁸ as well as other derivative frameworks including (R^4 anthraphos),²⁹ (R^4 POCOP),³⁰⁻³¹ (R^4 PCOP),³² (R^4 PSCOP),³³ (R^4 PC(sp³)P),³⁴⁻³⁷ (R^4 PNP),³⁸ (Phebox),³⁹⁻⁴⁰ (Pybox),⁴¹ and “pincer-crown ether” ligands ($^{15}\text{-crown-5NCOP}^{i\text{Pr}_2}$),⁴² among many others.

Complexes based specifically on the $[\text{Ir}(R^4PCP)]$ motif are exceptional catalysts for dehydrogenation of *n*-alkanes, with $[\text{Ir}(^{i\text{Pr}}R^4PCP)]$ achieving rates greater than 3700 TO hr⁻¹ in the *gas-phase* transfer dehydrogenation of pentane with propylene at 240 °C, and over 11500 TO hr⁻¹

¹ with *n*-octane as the substrate in solution-phase reaction.⁴³ Further, both [Ir(*i*Pr⁴PCP)] and [Ir(*t*Bu⁴PCP)] catalysts show high regioselectivity for dehydrogenation of the terminal position of *n*-alkanes.⁴³

In order to generate a heterogeneous dehydrogenation system based on such complexes, the binding environment around the metal center active site must be preserved upon immobilization. However, without an appropriate backbone tether, supporting these species on metal oxides such as alumina or silica results in the generation of a grafted iridium(III) center via oxidative addition of surface silanol groups.⁴⁴⁻⁴⁸ While these complexes were found to be highly active for olefin hydrogenation, apart from a few exceptions in the literature,³⁹⁻⁴⁰ the aforementioned pincer-ligated alkane dehydrogenation systems are based on Ir(I).

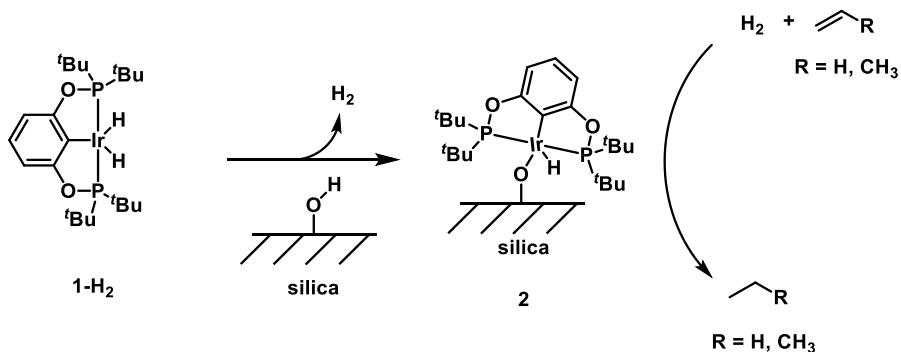


Figure 1. Mechanism for grafting of species **1-H₂** and **2** to generate a five-coordinate Ir(III) center that is capable of hydrogenation (right).

In order to work around this propensity for interaction with the surface, numerous efforts focusing on *tethering* pincer-metal complexes to surfaces via backbone modifications have been attempted. Previously heterogenized materials of this type have been based on pincer-metal complexes predominantly of palladium,^{23, 49-54} along with ventures into the immobilization of rhodium, nickel and ruthenium using *t*Bu⁴PONOP.⁵⁵⁻⁵⁶ Perhaps indicative of the difficulty associated with generating a truly stable, recyclable heterogenized species, it was found that

several of the immobilized pincer-palladium species served only as precursors for the active catalyst under the reaction conditions studied, dissociating and dissolving into the homogeneous phase at temperature.^{23, 52}

In contrast, pincer-iridium derivatives based on ligand frameworks with substitutions on the aromatic backbone *para*- to the iridium atom have been found to mitigate interaction with the surface and their immobilization resulted in catalysts which remained active for some time under reaction conditions.⁵⁷⁻⁵⁸ These efforts have resulted in systems based on heterogenized pincer-iridium catalysts which show activity for alkane dehydrogenation as well as alkane metathesis (as components of tandem systems).⁵⁷⁻⁵⁸ Of particular note is the immobilization of $[\text{Ir}(\text{C}_2\text{H}_4)(p\text{-}t\text{Bu}_2\text{PO}-t\text{Bu}^4\text{POCOP})]$ on a metal oxide toward this end, as the *para*- substituent in this case, through reaction with surface hydroxyl groups, generates a covalent tether (Figure 2).⁵⁷ The mechanism of this tethering reaction has been studied in detail and results in species of the form $[\text{IrL}(\equiv\text{SiO}-t\text{Bu}^4\text{POCOP})]$.⁵⁹

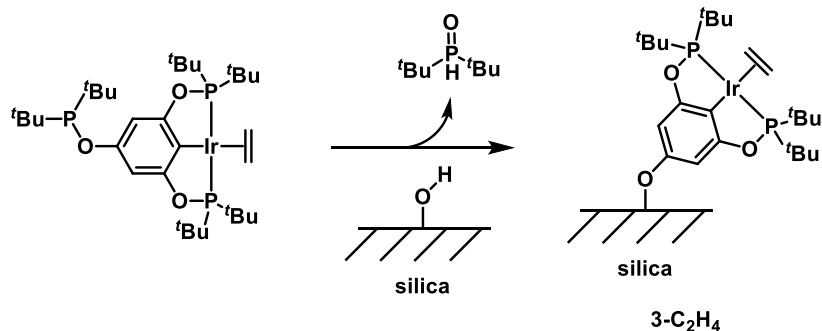


Figure 2. Formation of species **3-C₂H₄** with retention of iridium ligand environment from molecular precursor.

In previous work, we have expanded on these results by implementing a continuous-flow heterogeneous alkane dehydrogenation system based on silica-supported complexes $[\text{IrL}(\equiv\text{SiO}-$

$t\text{Bu}^4\text{POCOP})]$ ($\text{L} = \text{C}_2\text{H}_4$, **3-C₂H₄**; $\text{L} = \text{CO}$, **3-CO**). Such a system allows for the measurement of instantaneous turnover frequencies, as well as fine control over various reaction parameters including volumetric flow rate, temperature and pressure. It was shown that the catalysts studied remain stable under acceptorless thermocatalytic butane dehydrogenation conditions at temperatures up to 340 °C when at equilibrium conversion,⁶⁰ well above the temperatures at which solution phase catalysts have demonstrated stability.^{43, 60} Post-catalysis *ex situ* ^{31}P Magic-Angle Spinning (MAS) NMR analysis revealed that **3-C₂H₄** had converted to **3-CO**, and kinetic studies starting with **3-CO** as the catalyst showed that it was as effective as **3-C₂H₄** at temperatures above 300 °C. The mechanism of this ligand exchange, and the role of the carbonyl species in the decomposition pathways, could not be determined by *ex situ* studies. The activity of **3-CO** was unexpected given that CO blocks the reactive coordination site and thereby acts as a poison in alkane dehydrogenation systems based on pincer-iridium.

In this work, we seek to study this catalytic system under kinetic conditions, far from alkane/alkene equilibrium, and to determine the various iridium-containing species generated on the surface as a function of temperature. Of particular import was the study of the role of carbon monoxide, and how it influences the conversion between these species. Using *operando* Diffuse Reflectance Infrared Fourier-Transform Spectroscopy (DRIFTS), complete conversion of **3-C₂H₄** to **3-CO** was observed during reaction conditions. Starting with $[\text{IrClH}(\equiv\text{SiO}-t\text{Bu}^4\text{POCOP})]$ (**3-HCl**) also led the generation of **3-CO** *in situ* (Figure 3). Several intermediate CO-containing iridium decomposition products were characterized, and the temperatures of decomposition associated with formation of these products were elucidated.

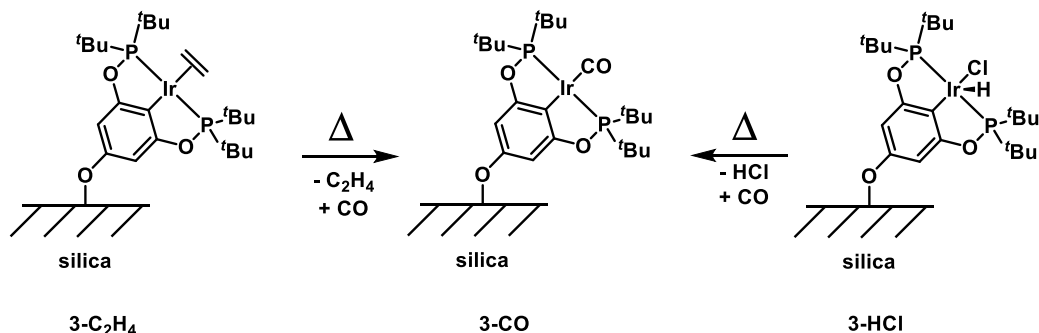


Figure 3. Structures of the complexes used in this work. Conversion of **3-C₂H₄** and **3-HCl** to **3-CO** is observed in this work. **3-CO** remains catalytically active and stable under reaction conditions at 300 °C.

This apparent role of **3-CO** as a thermodynamic sink at reaction temperatures, along with spectrokinetic measurements discussed here, point to a complicated role played by CO in this reaction system, in which it serves both as a catalyst inhibitor by removing iridium from the catalytic cycle, as well as a protector by minimizing interaction of the iridium center with the silica surface, thus inhibiting its decomposition and increasing its maximum thermal stability. For this reason, carbon monoxide, the formation of which was initially considered an unavoidable nuisance in this system, should have its role reconsidered as a potentially beneficial additive in catalyst systems based on surface-supported metal complexes.

2. Experimental Methods

2.1 Catalyst Preparation

All chemical syntheses and material preparations were performed under an argon atmosphere unless otherwise noted. Molecular complexes $[\text{Ir}(\text{C}_2\text{H}_4)(p\text{-}t\text{Bu}_2\text{PO-}t\text{Bu}_4\text{POCOP})]$, $[\text{Ir}(\text{CO})(p\text{-}t\text{Bu}_2\text{PO-}t\text{Bu}_4\text{POCOP})]$ and $[\text{IrClH}(p\text{-}t\text{Bu}_2\text{PO-}t\text{Bu}_4\text{POCOP})]$ were synthesized, and supported catalysts **3-L** (L = C₂H₄, CO, HCl) prepared, according to previously established procedures.⁶⁰

Calcination of silica support material was carried out under dry air in a 6.4 mm outer diameter (OD) quartz tube reactor with an expanded section of 12.5 mm OD packed with quartz wool to hold the catalyst powder in place. After calcination, the powder was flushed with helium prior to being brought into an argon glovebox for further use. Supports were calcined to 550 °C with a ramp rate of 2 °C/min and a hold of five hours at temperature.

2.2 Gas-phase Continuous-flow Catalytic Data

Plug-flow reactions were carried out in a 6.4 mm outer diameter (OD) quartz tube reactor with an expanded section of 12.5 mm OD packed with quartz wool to hold the catalyst powder in place. The reactor was packed with supported catalyst under argon atmosphere, sealed with valves prior to connection to the gas-flow manifold, and connected under inert gas flow. The reactor was placed inside a resistively heated ceramic furnace with external temperature control, and the catalyst bed temperature was measured with a K-type thermocouple placed in direct contact with the catalyst bed.

Operando DRIFTS measurements were performed using a Nicolet iS50 FTIR spectrometer equipped with liquid nitrogen-cooled MCT/A detector and a Harrick HVC-DRM5 high temperature reaction chamber inside a Praying Mantis accessory. The reaction chamber temperature was calibrated with a wire thermocouple inserted into the catalyst bed under a closed dome through one of the inlets with no gas flow. The spectral resolution was set to 2 cm⁻¹ and 64 scans were averaged for each spectrum shown. An atmospheric suppression algorithm was utilized to eliminate signals arising from atmospheric water and carbon dioxide inside the instrument sample compartment but outside the reactor chamber.

In a typical kinetic experiment in the quartz tube plug-flow reactor, 5 mg of iridium complex was supported on 150 mg of support via incipient wetness impregnation, and the

resulting material was loaded into the reactor. In a typical spectrokinetic experiment in the DRIFTS reactor, only 30 mg of the resulting material was packed into the sample cup per experiment. The surface of the powder bed was flattened with the Harrick sample packing tool to achieve a smooth surface.

Butane (Airgas, 99.99%), 1-butene (Matheson, 99%), ethane (Matheson, 99.999%), ^{13}CO (99%, Sigma-Aldrich) and 1% CO/Helium (Praxair) were used as received. Helium (Praxair, 99.999%) was passed through an on-stream oxygen and moisture trap. Reaction products were analyzed using an Agilent 7890B GC instrument equipped with a GS-GASPRO capillary column (0.32 mm \times 60 m) fitted with a splitter plate connected to a flame ionization detector and an Agilent 5977A mass spectrometer. Unless stated otherwise, all experiments were carried out at 1.27 atm total pressure by throttling a needle valve located downstream from the reactor. Gas flow rates reported were measured at room temperature and pressure.

2.3 Processing of DRIFTS Spectra and Peak Fitting

Raw reflectance data obtained from DRIFTS experiments was converted to Kubelka-Munk units,⁶¹⁻⁶² which serve as an analogue for units of absorbance in diffuse reflectance spectroscopy using the following formula:

$$F(R_{\infty}) = \frac{(1 - R_{\infty})^2}{2R_{\infty}}$$

$$R_{\infty} = R_{\text{sample}}/R_{\text{ref}}$$

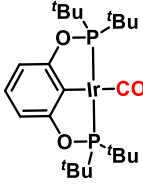
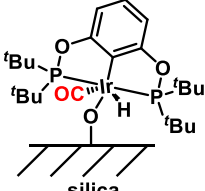
R_{∞} is the absolute reflectance, R_{sample} is the measured reflectance of the sample and R_{ref} is the measured reflectance of a standard defined to possess a diffuse reflectance of unity, chosen in this work to be KBr.

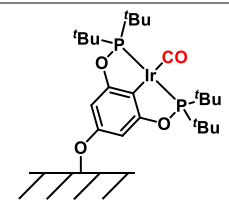
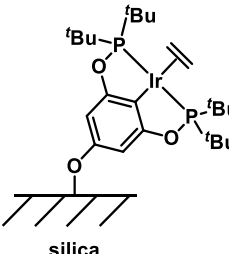
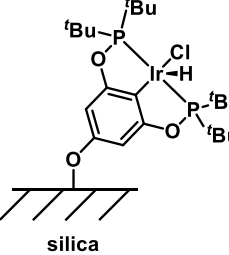
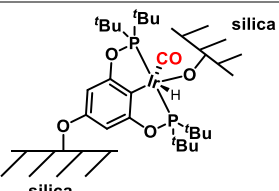
Deconvolution and peak fitting of background-subtracted, spline-corrected spectra was carried out using Fityk software.⁶³ Fourier Self-Deconvolution⁶⁴ (FSD) performed in Origin⁶⁵ allowed for determination of peak positions in authentically supported carbonyl species **3-CO** (Figure S1). Peak parameters were determined by allowing three model Voigt functions to relax to an IR spectrum obtained from an authentic, freshly supported sample **3-CO**. Spectral features were then fit for the remainder of analyzed spectra conserving these parameters. All fits were performed by minimizing the weighted sum of the square residuals using the Levenberg-Marquardt method.⁶⁶⁻⁶⁷

3. Results and Discussion

3.1 Freshly Prepared Catalysts

Table 1. Summary of catalyst species and associated carbonyl absorbance frequencies observed in this work. All spectra collected at room temperature.

Species	ν_{CO} (cm ⁻¹) this work	ν_{CO} (cm ⁻¹) references
 <p>1-CO</p>	<p>1932 s^a</p> <p>1954 s, 1924 w^b</p>	<p>1934^{c,46}</p> <p>1949^{d,46}</p> <p>1952, 1924^{b,46}</p>
 <p>2-CO</p>	<p>2024 s^b</p>	<p>2026^{b,46}</p>

 <p>silica</p> <p>3-CO</p>	1948 s, 1958 m, 1930 w ^b	1945 ^{e,57}
 <p>silica</p> <p>3-C₂H₄</p>	none	
 <p>silica</p> <p>3-HCl</p>	none	
 <p>silica</p> <p>4-CO</p>	2043 s ^b	-
Decomposition Product 1	1970	-
Decomposition Product 2	1978	-

s strong, m moderate, w weak relative to bands within the same region of the spectrum.

^aSolid-phase, sublimated/recrystallized on zinc selenide IR cell surface.

^bSupported on silica.

^cSolid-phase, CsI pellet.

^dSolution-phase, pentane solvent. This assignment is also comparable to that seen with **3-CO**, which contains an identical iridium coordination sphere in the vicinity of silica.

^eSupported on γ -alumina.

Species **3-L** (L = C₂H₄, CO, HCl) were prepared following literature procedures,⁶⁰ and freshly supported materials were characterized via DRIFTS. Upon supporting molecular

complexes with the *para*-phosphinite moiety, reaction with surface silanol groups results in a covalent tether immobilizing the complex on the surface. While at room temperature a small amount of complex remained physisorbed instead of chemisorbed, upon heating the material all of the catalyst quickly reacted to afford the covalent tether necessary for immobilization.^{59, 68}

In the case of freshly supported authentic **3-CO**, three distinct features were observed at 1930, 1948 and 1958 cm^{-1} by DRIFTS (Figure 4). **1-CO** is reported to have a stretch of 1949 cm^{-1} when in pentane solution, absent any intermolecular interactions.⁴⁶ The feature at 1948 cm^{-1} observed in this work, by analogy, is likely the “parent” feature attributable to the silica-supported 4-coordinate Ir(I) of **3-CO**. The presence of this feature demonstrates that silica-supported complexes of this type stabilize the coordination sphere found in solvated iridium analogues even when effectively in the solid phase, and truly are site-isolated and unique in this capacity by comparison to bulk molecular crystals. The residual features are shifted due to either intermolecular or surface interactions. For instance, the feature at 1930 cm^{-1} is comparable to that observed at 1934 cm^{-1} in solid-phase in previous work,⁴⁶ or that observed at 1932 cm^{-1} when recrystallized on zinc selenide in this work. These signals likely arise from hydrogen bonding interactions in the crystal structure of such derivatives which serve to decrease the CO bond order. The origin of the remaining signal at 1958 cm^{-1} is unclear, but it may arise from secondary interactions between the pincer-iridium complex and the silica surface.

A blue-shifted peak at 2043 cm^{-1} is indicative of a CO ligand bound to a six-coordinate Ir(III) center.⁴⁶ This is consistent with an interaction between iridium and the surface arising from oxidative addition of a silanol group, possibly giving rise to a structure like **4-CO** in which the complex is still also tethered to the surface through the backbone.

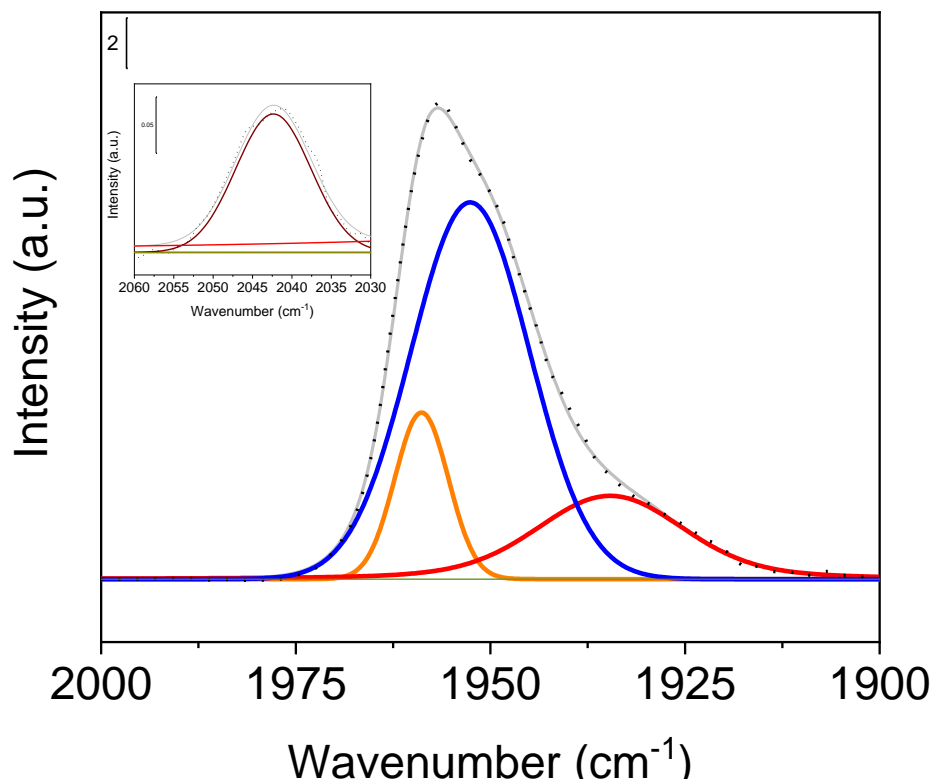


Figure 4. DRIFTS spectrum of **3-CO** taken at 200 °C. Peak fittings of the 1930 cm^{-1} (-), 1948 cm^{-1} (-), 1958 cm^{-1} (-) and 2043 cm^{-1} (-) bands are shown along with the sum (-) superimposed over the experimental data.

Pincer-ligated iridium species lacking the covalent tether at the *para*-position were susceptible to sublimation. Even the oxidative addition of a silanol group to iridium was insufficient to keep the complex tethered under mild heating. Upon heating to 200-240 °C, species of type **2-L**, including **2-C₂H₄**, were observed by DRIFTS to convert to **2-CO** and then to sublime off the surface and redeposit on the interior of the reaction chamber resulting in a band observed at 1932 cm^{-1} corresponding to molecular complex, coating present reactor cold spots (Figure S2). The same experiment repeated with other pincer-ligated species $[\text{Ir}(\text{}^{i\text{Pr}}_4\text{PCP})(\text{C}_2\text{H}_4)]$ and $[\text{Ir}(\text{}^{i\text{Pr}}_4\text{Anthrophos})(\text{C}_2\text{H}_4)]$ ⁶⁹ also resulted in their sublimation at ca. 240 °C. In contrast, no iridium complex sublimation was observed with the covalently anchored analogues **3-L**.

3.2 Catalyst Speciation under Reaction Conditions

By analogy to catalytic dehydrogenation performed previously with **3-C₂H₄** and **3-CO** at equilibrium conditions,⁶⁰ species **3-L** (L = C₂H₄, CO, HCl) were used in this work to perform alkane dehydrogenation in a continuous-flow reactor under kinetic conditions at very short residence times. The equilibrium constant for butane dehydrogenation as a function of temperature was calculated from standard enthalpies and entropies of formation for butane, all possible linear butenes and hydrogen at temperatures tested, and determination of the approach to equilibrium $\eta = Q/K_{eq}$ (Figure S3) confirms that even at the very highest temperatures, equilibrium is not reached ($\eta < 0.4$).

Supported ethylene complex **3-C₂H₄** has previously been observed to convert to carbonyl species **3-CO** at elevated temperatures under butane, and this species was subsequently observed to be stable up to 340 °C, achieving dehydrogenation rates of ca. 80 TO hr⁻¹ at this temperature. The distribution of products arising from dehydrogenation of butane was observed to follow thermodynamic ratios under all conditions and residence times tested, with approximately 20% terminal olefin, 1-butene.⁶⁰

In this work, all species **3-L** (L = C₂H₄, CO, HCl) were observed to convert to **3-CO** at elevated temperatures as well, indicating that this species is an accessible thermodynamic sink. Generally, shorter residence times lead to higher observed turnover frequencies as there is less competition from the back reaction, in this case hydrogenation. However, in the case of catalyst decomposition, shorter residence times also preclude equilibration, showing more clearly inhibition of catalytic activity which would be masked at equilibrium conditions. Thus, a direct comparison of this work to previous work must take this factor into account. Turnover

frequencies for **3-L** at 340 °C were observed to be ca. 124 hr⁻¹ (**3-C₂H₄**), ca. 60 hr⁻¹ (**3-CO**), and 140 hr⁻¹ (**3-HCl**). The amount of complex used in these experiments was very low, typically less than 1 mg molecular precursor, so some variation in the calculated rates is expected. Spectroscopically, all supported materials followed nearly identical evolution and decomposition pathways and the complex speciation under reaction conditions, as well as subtle differences arising therein as a result of starting complex, is the primary focus of this work. (The source of CO under reaction conditions is explored below in Section 3.3.)

Changes in the catalyst material under operando reaction conditions were studied by subjecting samples to a temperature ramp from 200 – 440 °C under butane dehydrogenation conditions at low conversion in the DRIFTS reactor (Figure 5a). As mentioned, short residence times were chosen for all reactions to maintain low conversion and to ensure that the reaction was far from equilibrium, eliminating competition from the reverse reaction of hydrogenation of the product olefin.

Starting from **3-C₂H₄**, generation of the CO complex, as evidenced by the growth of the bands at 1948 cm⁻¹ and 1958 cm⁻¹ (Figure 5b) was observed at temperatures as low as 170 – 220 °C. These features continued to increase in intensity as a function of temperature up to 300 °C. During each isothermal hold period, at temperatures from 240 – 300 °C, catalyst activity increased throughout the hold, indicating that achieving steady-state is not instantaneous. For this reason, and since accurate characterization of high temperature decomposition was of particular interest in these experiments, an isothermal hold at 280 °C was incorporated into these experiments prior to ramping to higher temperatures, since the catalyst was observed to be stable, as evidenced by no changes in the carbonyl bands present.

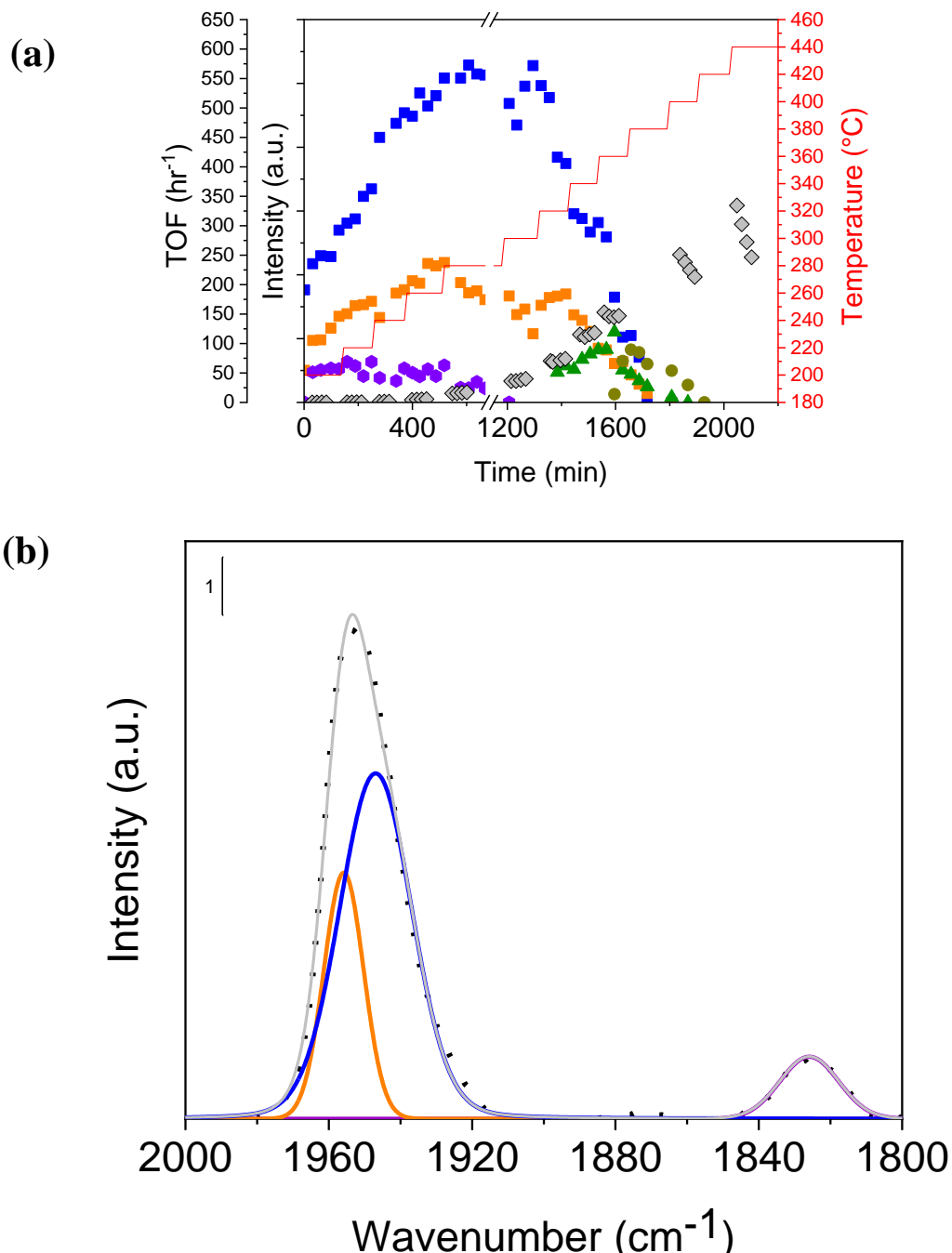
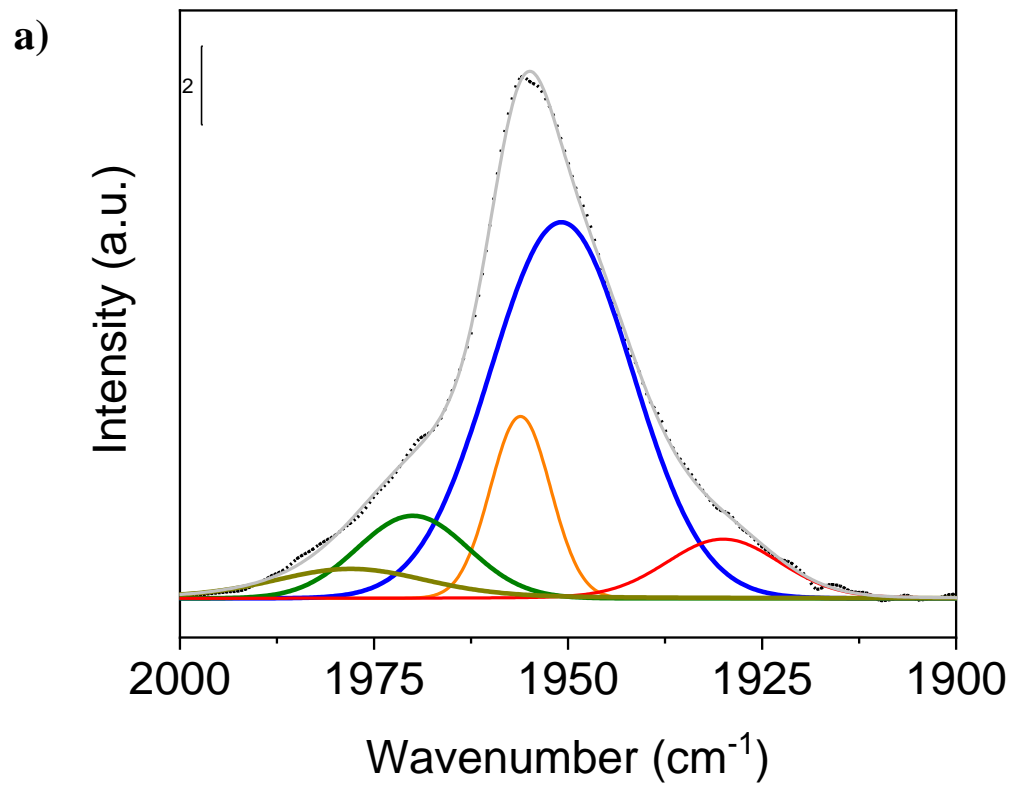


Figure 5. (a) Butene turnover frequencies (\diamond) overlaid with integrations of IR bands 1948 cm⁻¹ (\blacksquare), 1958 cm⁻¹ (\blacksquare), 1970 cm⁻¹ (\blacktriangle), 1978 cm⁻¹ (\bullet) and 1823 cm⁻¹ (\bullet) for butane dehydrogenation over **3-C₂H₄**. Note that the reaction was held at 280 °C for ca. 700 minutes, as indicated by the break in the x-axis at 700 minutes. $\dot{V}_{\text{total}} = 20 \text{ mL min}^{-1}$, $P_{\text{butane}} = 0.32 \text{ atm}$, $P_{\text{He}} = 0.95 \text{ atm}$, $P_{\text{total}} = 1.27 \text{ atm}$. (b) DRIFTS spectrum of **3-C₂H₄** at 220 °C under butane dehydrogenation conditions (black points). Peaks fitting the 1948 cm⁻¹ (\blacksquare), 1958 cm⁻¹ (\blacksquare), and 1825 cm⁻¹ (\blacksquare) bands are shown along with the sum (--) superimposed over the experimental data.

At lower temperatures, a peak was observed at 1823 cm^{-1} . This peak appeared ca. $180 - 200\text{ }^{\circ}\text{C}$ and disappeared by $300\text{ }^{\circ}\text{C}$. The position of this peak is highly suggestive of the CO stretching seen with bridging carbonyl moieties, but it does not match those observed in iridium nanoparticles.⁷⁰ This peak was not observed when starting with **3-CO** or **3-HCl**, and the relatively high lability of the ethylene ligand may be related to its formation. A possible origin for this peak may be interaction between two or more iridium centers following ethylene ligand loss, and subsequent CO addition. By $300\text{ }^{\circ}\text{C}$, the peak disappeared, indicating that this transient species decomposed to some other IR-silent species. Ramping the catalyst temperature back down to room temperature did not result in the return of this species, indicating irreversible conversion of this species at higher temperature.

Upon further increasing the reaction temperature above $320\text{ }^{\circ}\text{C}$, the intensity of the carbonyl bands at 1948 and 1958 cm^{-1} decreased. Above this temperature, the rate of reaction also declined as a function of time on stream, with a more rapid decline at higher temperatures where the carbonyl peaks were smaller. By $340\text{ }^{\circ}\text{C}$, two new bands were observed in the carbonyl region at 1970 cm^{-1} and 1978 cm^{-1} (Figure 6a). Continuing to increase the temperature above $340\text{ }^{\circ}\text{C}$ led to continued growth in the 1978 cm^{-1} band while the band at 1970 cm^{-1} reached a maximum and then decreased in intensity to zero. By $400\text{ }^{\circ}\text{C}$, the former was the only remaining feature (Figure 6b). Maintaining this temperature or increasing it further led to complete loss of all carbonyl signals. No new CO signals were observed, even following dosing with CO after cooling the sample to room temperature to rule out dissociation of CO with a shifting thermal equilibrium, indicating the formation of a thermodynamically stable IR-silent decomposition product at this temperature. Interestingly, even at longer reaction times, the speciation of iridium carbonyl complexes on the surface arising from heating and decomposition,

as determined via DRIFTS, is identical independent of whether alkane is present in the feed or not.



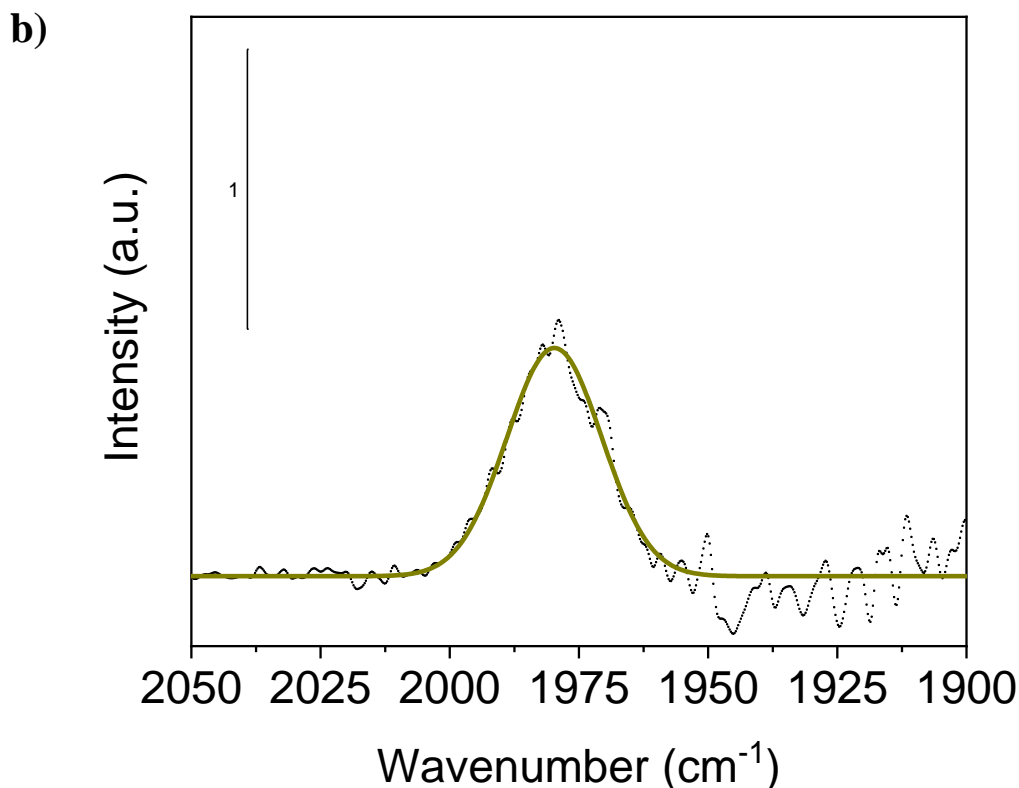


Figure 6. (a) DRIFTS spectrum of **3-C₂H₄** at 320 °C under butane dehydrogenation conditions (**black** points). Peaks fitting the 1930 cm⁻¹ (-), 1948 cm⁻¹ (-), 1958 cm⁻¹ (-), 1970 cm⁻¹ (-) and 1978 cm⁻¹ (-) bands are shown along with the sum (-) superimposed over the experimental data. (b) DRIFTS spectrum of **3-C₂H₄** at 380 °C under butane dehydrogenation conditions. Peak 1978 cm⁻¹ (-) band is shown superimposed over the experimental data. No other features in the carbonyl region are present.

Performing an identical temperature ramp with **3-CO** resulted in a nearly identical kinetic profile (Figure S4). In an attempt to further probe the effect of initial catalyst structure on decomposition routes, **3-HCl** was subjected to a similar temperature ramp under dehydrogenative conditions (Figure S5), and it was observed that it also converts to CO species at relatively low temperatures. Above 280 °C, all three reactions resulted in generation of **3-CO** and displayed nearly identical reaction profiles.

Reaction rates measured when starting with **3-HCl** and **3-CO** were significantly higher at temperatures above 300 °C than with **3-C₂H₄**, consistent with the decomposition of some of **3-C₂H₄** to an out-of-cycle iridium species upon deposition. Notably, efforts have previously focused on making use of olefin-bound precatalysts such as **3-C₂H₄** for alkane dehydrogenation studies, but starting with **3-HCl** or **3-CO**, species that are inactive at low temperatures, ultimately gives greater activity. Dehydrogenation starting with **3-C₂H₄** is observed to result in lower TOFs than either **3-HCl** or **3-CO**, in part due to interaction between iridium centers with concurrent loss of ethylene (1823 cm⁻¹ in Figure 5b). At temperatures above 320 °C, progressive loss of CO stretching bands at 1930, 1948 and 1958 cm⁻¹ was observed coinciding with a gradual loss of activity for butane dehydrogenation.

3.3 Role and Origin of Carbon Monoxide

The characteristic differences between the present work and previously explored analogous solution-phase chemistry^{25, 27} are higher temperatures and the presence of a carbonyl-bound catalytic resting state. While the chemistry of pincer-iridium carbonyl complexes has been explored in some detail,⁷¹⁻⁷⁵ these complexes have generally been treated as quintessentially inactive toward alkane dehydrogenation, at least at the temperatures accessible by these catalysts. It is thus surprising that **3-CO** appears to perform dehydrogenation rather effectively in this work, albeit at rates much less than CO-free pincer-iridium species. The CO bound species are stable at relatively high temperatures, however, both in solution and on supports. We therefore considered that the CO ligand may play a role both as catalyst inhibitor stabilizer.

If CO promotes stability and prevents (or delays) decomposition, then cofeeding CO should enhance this effect. To test this, 500 ppm CO was co-fed along with butane to the reactor

and the results were compared against a control reaction in which no co-fed CO was present (Figure 7). In the control experiment with no co-fed CO, the onset of features at 1970 and 1978 cm^{-1} , associated with carbonyl-bound decomposition products, were observed to begin growing in at 320 °C (Figure 7a). By comparison, when CO was co-fed, the onset of these features was delayed by 20 °C to 340 °C (Figure 7b). The ratio of the features at 1948 and 1958 cm^{-1} associated with **3-CO**, was also significantly different at all temperatures. The delay in decomposition is evidence of a small but measurable impact on stability under higher partial pressures of CO when it is co-fed, and the variance in ratios of bands is indicative of a significant impact of CO on surface speciation. Further, while the signals corresponding to the two decomposition products were observed to grow in together in the control experiment with no co-fed CO, the generation of the longest-lived IR-visible decomposition product (1978 cm^{-1}) was slowed at higher temperatures, as evidenced by the fact that this band does not begin to grow in until the band at 1970 cm^{-1} reached a maximum at ca. 380 °C. From this it seems that an increased pressure of CO also serves to protect this decomposition product (1970 cm^{-1}) from undergoing further decomposition as well, consistent with a scheme in which this species is an intermediate along the catalyst decomposition pathway.

The CO co-feed has the effect of reducing overall catalytic activity significantly, from 14 TO hr^{-1} to 0.4 TO hr^{-1} at 300 °C. This much lowered activity at a low partial pressure of CO implies that loss of CO from the carbonyl complex is reversible and necessary for catalytic activity, and that dehydrogenation follows a catalytic cycle analogous to that in solution-phase reactions. Work focusing on optimizing a system in which CO is cofed to reap the benefits of increased selectivity while mitigating catalyst inhibition is currently underway.

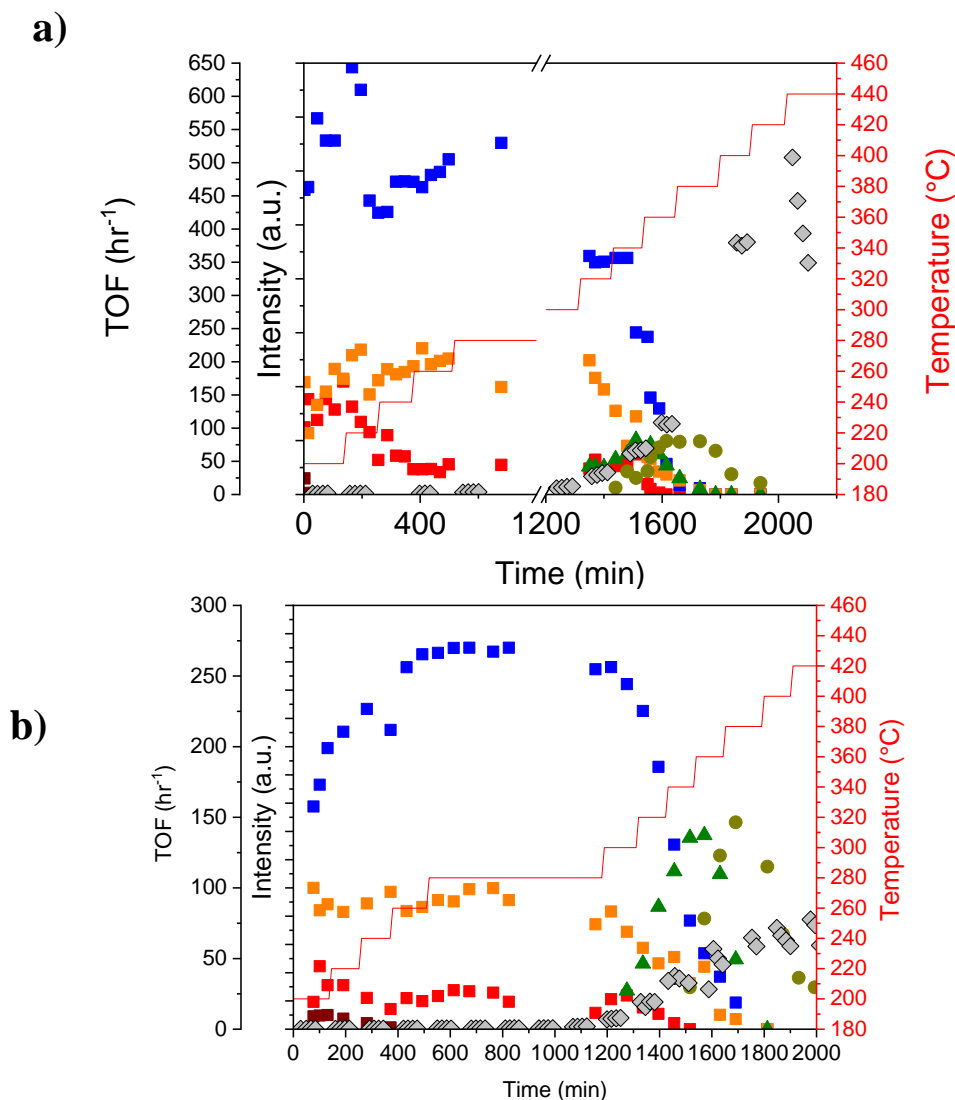


Figure 7. Butene turnover frequencies (\diamond) overlaid with integrations of IR bands 1930 cm^{-1} (\blacksquare), 1948 cm^{-1} (\blacksquare), 1958 cm^{-1} (\blacksquare), 2043 cm^{-1} (\blacksquare), 1970 cm^{-1} (\blacktriangle), and 1978 cm^{-1} (\bullet) for butane dehydrogenation over **3-CO**, (a) with and (b) without 500 ppm CO co-feed. Note that the reaction was held at $280\text{ }^{\circ}\text{C}$ for ca. 700 minutes in part (a), as indicated by the break in the x-axis at 700 minutes. $\dot{V}_{\text{total}} = 20\text{ mL min}^{-1}$, $P_{\text{butane}} = 0.32\text{ atm}$, $P_{\text{He}} = 0.95\text{ atm}$, $P_{\text{total}} = 1.27\text{ atm}$.

In order to determine the likely processes by which carbon monoxide is produced in this system, the sources of both carbon and oxygen must be considered. The three known possible sources of oxygen in the system are: (i) water, either physisorbed or present as chemisorbed water in the form of surface silanol groups; (ii) linker groups of the pincer ligand; or (iii) the byproduct of the phosphine oxide leaving group, di-*tert*-butylphosphine oxide, produced upon condensation of the catalyst precursor with a silanol group.^{57, 59-60} Access to the oxygen in the

linker arms of the pincer ligand would necessitate decomposition of the pincer ligand itself, resulting in an ever-decreasing catalytic activity even at low temperatures, which is not observed. If the oxygen was derived from byproduct phosphine oxide only, then upon consumption of this material, carbonyl production should cease – given that one equivalent of phosphine oxide is produced for every equivalent of supported catalyst,⁵⁹ this would allow for a total of precisely one equivalent of CO being produced and, upon complete conversion of the starting complex to **3-CO**, catalytic activity should be observed to drop even at low temperatures as CO escapes the system, which is not observed. With regard to water present, while the powders are calcined prior to use and the reactor dried at elevated temperature prior to packing of supported catalyst powder, DRIFTS scans of freshly supported catalyst reveal the presence of perturbed silanol groups at wavenumbers lower than that corresponding to site-isolated silanol OH groups (indicating presence of chemisorbed water), consistent with the presence of adsorbed water interacting with these groups (Figure S7).

The likely source of carbon seems obvious when there is a steady feed of butane in the system, but the fact that CO is generated even under helium flow (as evidenced by presence of carbonyl-containing species, Section 3.2) indicates that at the very least one other carbon source is also available. Various sources of carbon may be proposed, including the *tert*-butyl groups of the pincer ligand, the *tert*-butyl groups of the phosphine oxide generated upon tethering,⁵⁹ CO contamination in any of the reagent gas streams used, as well as trace carbonaceous impurities in the silica. Derivation of carbon from the pincer-ligand is unlikely for the same reason invoked for derivation of oxygen from the same – this would necessitate decomposition of the ligand itself, leading to ever-decreasing catalytic rates even at lower temperatures, which is not observed. In contrast, C-H activation of *tert*-butyl groups found on di-*tert*-butylphosphine oxide

would not decrease catalytic rates due to catalyst decomposition, and would allow for eight equivalents of CO to be formed per molecule of phosphine oxide and, thus, per pincer-iridium complex (since the ratio of these is 1:1).

In order to probe the source of CO further, labeling studies were carried out with **3- ^{13}CO** . Since CO dissociation must occur in order for catalysis to take place (*vide supra*), if the autogenesis of CO continues throughout the course of the reaction, and it is assumed that there are no highly populated IR-invisible resting states present, exposure of **3- ^{13}CO** to high temperature should lead to replacement of the ^{13}CO ligand with unlabeled CO. Given that butane is one possible carbon source, the rate of CO exchange, and thus ^{13}CO loss, should be at least partly controlled by the abundance of alkane available in the system. Prior to increasing the temperature to 300 °C, the catalysts were dried in situ at 100 °C under flow of the chosen gas until the IR spectra remained unchanged – note that at this temperature no CO production or exchange was observed when CO was not cofed - indicating complete desorption of all weakly bound water and deposition solvent, benzene.

In the ^{13}CO labelled samples, two peaks were seen at low temperature. The primary peak at 1908 cm^{-1} corresponded to the shift in the feature arising from bands at 1948 and 1958 cm^{-1} peak in the unlabeled complex, and a small, broad band at 1999 cm^{-1} arose from the shift of the band at 2043 cm^{-1} for **4-CO**. Both of these shifts are predicted by the change in reduced mass as a result of isotopic labeling of the ^{13}CO ligand.⁴⁶ A difference in response factors was noted between the labelled and unlabeled peaks, likely due to optical or cross-section effects in the DRIFTS experiment arising from the fact that diffuse reflectance spectra are only semiquantitative when comparing peaks at different frequencies. This difference in apparent

response factors was corrected for by applying an empirically derived correction coefficient (Figure S7).

The rate of loss of **3-¹³CO** and the rate of growth in of **3-CO** were monitored using in situ DRIFTS (Figure 8, S8-S9, respectively) under various gas flows at 300 °C using the maximum observed CO absorptions for both of 1908 cm⁻¹ (**3-¹³CO**) and 1958 cm⁻¹ (**3-CO**). At this temperature, no other iridium species were expected. Plotting the calculated surface concentrations (nmol m⁻²) against time reveals information about the rates associated with replacement of bound ¹³CO with unlabeled CO, and thus conversion of **3-¹³CO** to **3-CO** (Figure 8).

The rate constant for the initial decline in **3-¹³CO** concentration at 300 °C when at very early reaction times (ca. 0-10 min), as derived from plotting the natural logarithm of this concentration versus time, was found to be identical regardless of whether the reaction atmosphere was butane, ethane, 1-butene or helium, indicating a shared mechanism of CO production at early times on stream ($k = -0.017 \text{ min}^{-1}$). Under helium flow, about 20 minutes after the reaction began, the rate of isotopic exchange slowed down relative to the other hydrocarbon gas flows and by about 170 minutes, exchange had stopped and the ¹³CO signal remained constant. These results suggest that di-*tert*-butylphosphine oxide is the likely initial source of carbon leading to the production of the unlabeled CO. In the case of the run with helium flow, these sources are exhausted by about 170 min and no further unlabeled CO is produced; this argues against the pincer ligand itself being a carbon source. In the case of hydrocarbon flow, the hydrocarbon acts as a carbon source although more slowly than the initial source. Ethane appears to be a somewhat less effective source than butane, possibly because its dehydrogenation (followed by hydration and decarbonylation) is thermodynamically less

favorable. The decarbonylation reaction observed here should be limited by the amount of oxygen present in the system which is finite. However, the expected surface silanol density is at least 1-2 orders of magnitude greater than the amount of catalyst present.⁷⁶ For example, catalyst activity was maintained even for very long time on stream with no activity loss observed over 33 days, with approximately 36,000 total turnovers (Figure S10).

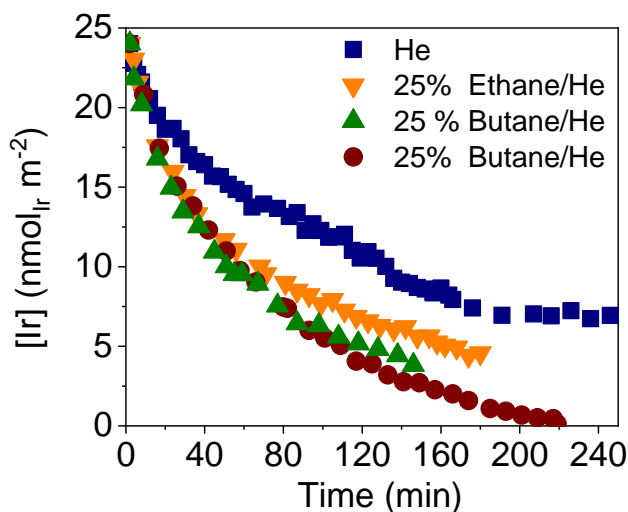


Figure 8. Plots of the concentration of ^{13}CO labeled species in the conversion of $3\text{-}^{13}\text{CO}$ to 3-CO versus time under helium (■), 25% ethane in helium (▼), 25% butane in helium (●), 25% 1-butene in helium (▲). $n_{\text{cat}} = 1.34 \mu\text{mol}$, $\dot{V}_{\text{total}} = 40 \text{ mL min}^{-1}$, $P_{\text{alkane}} = 0.32 \text{ atm}$, $P_{\text{He}} = 0.95 \text{ atm}$, $P_{\text{total}} = 1.27 \text{ atm}$, $T = 300 \text{ }^{\circ}\text{C}$.

The role of carbon monoxide in this catalytic system is twofold. On the one hand, it serves as a poison in the sense that it inhibits catalytic activity by comparison to a (hypothetical, but presently impossible) system operating at elevated temperatures in which there is no carbon monoxide present. This is the primary reason why the turnover frequencies associated with acceptorless dehydrogenation using species of type **3-L** are consistently lower than solution-phase analogues by 1-2 orders of magnitude.

On the other hand, the presence of carbon monoxide enhances long-term stability. Carbon monoxide may prevent formation of catalytically inactive Ir(III) products formed by oxidative

addition of surface silanol moieties. Thus it may be viewed as a promoter for, or a protector of, activity, mitigating the strong interaction with the surface which inhibits catalysis and also ultimately leads to decomposition. These, as well as other, relevant catalyst transformation pathways are shown in Figure 9. Moreover, the catalytic effectiveness of the CO complex also allows it to act as an air-stable precatalyst, making this system more convenient and amenable to scale-up.

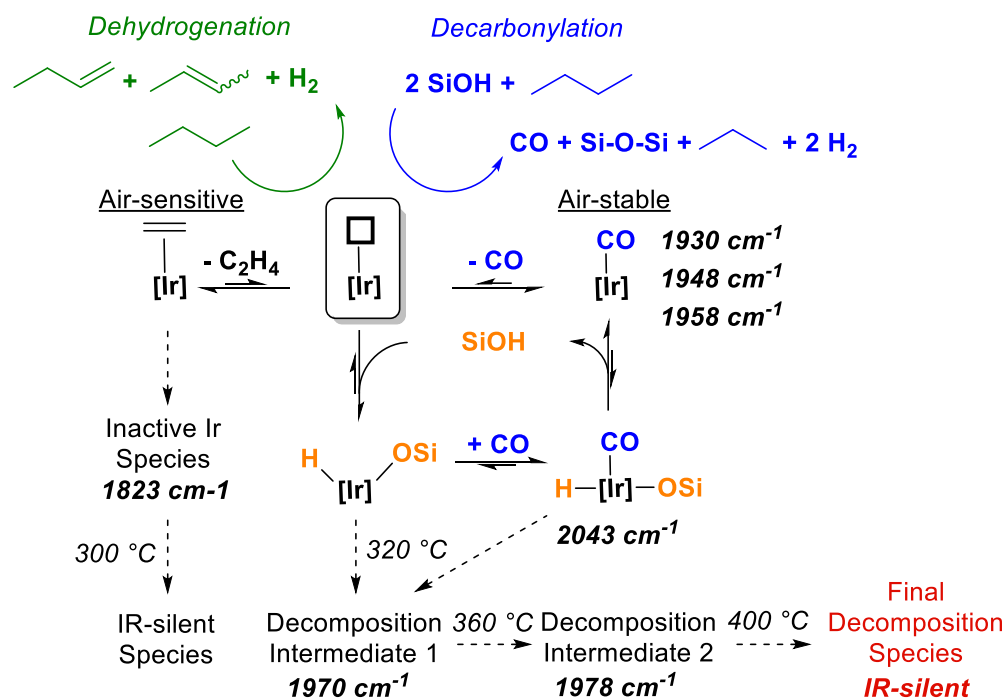


Figure 9. Reaction scheme detailing catalyst transformations (Dashed arrows correspond to proposed decomposition pathways), along with associated CO stretch wavenumbers and relevant reaction temperatures. $[\text{Ir}] = \mathbf{3}$.

To explore a heterogeneous system absent of carbon monoxide, the results in this work indicate that various more exotic measures must be taken in order to remove the amount of accessible oxygen present. Strategies such as silanol-capping, making use of pincer frameworks that contain less/no oxygen, and using plug flow reactors composed of a material other than quartz are all currently under investigation for future work.

4. Conclusions

In this work, DRIFTS was used to determine catalyst speciation of supported pincer-iridium complexes under dehydrogenative conditions at temperatures 60 °C higher than previous solution-phase or molecular-phase analogues. It is found that both Ir(I) and Ir(III) supported species are efficient for CO generation, resulting in conversion to the CO-bound supported complex **3-CO** beginning at relatively low temperatures of 150-200 °C. The carbon source for the CO can apparently be the phosphine oxide byproduct of the tethering reaction, but in the presence of added alkane that becomes the major carbon source, likely via dehydrogenation/hydration/decarbonylation. Independent of the source of CO, the carbonyl complex is stable up to 300 °C, above which decomposition proceeds through two carbonyl-containing species before conversion to an IR-silent material. Carbon monoxide appears to serve a role protecting the catalyst from deactivation by iridium-bound surface silanol groups. The description of the decomposition pathways accessed in this system will serve to inform future catalyst design, including making use of alternate frameworks and tethers to further increase catalyst thermal stability.

Supporting Information

Overlay of Fourier Self-Deconvolution (FSD) and DRIFTS spectra of freshly prepared **3-L**; Sublimation and deposition of untethered pincer-iridium complex **1-CO**; Calculation of approach to equilibrium; Comparison of kinetics in the Harrick cell and a quartz tube plug-flow reactor with **3-CO**; Kinetic and spectroscopic profile of dehydrogenation reaction using **3-HCl**; Absence of catalytic activity with $[\text{Ir}(\text{COD})\text{Cl}]_2/\text{SiO}_2$; DRIFTS OH region showing effect of drying freshly supported catalyst, consistent with water adsorption; Derivation of correction coefficient in ^{13}CO labeling studies; Plots exploring the rate of formation of **3-CO** in ^{13}CO exchange reactions; DRIFTS spectra indicating rapid CO exchange at **4- ^{13}CO** to generate **3-CO**; Long-term stability test of **3-CO**

Author Information**Corresponding Author**

*F.E.C.: tel, +1 848 445 5558; e-mail, fuat.celik@rutgers.edu.

ORCID

Boris Sheludko: 0000-0003-4652-4531

Cristina F. Castro: 0000-0003-0808-3376

Alan S. Goldman: 0000-0002-2774-710X

Fuat E. Celik: 0000-0002-5891-6375

Notes

The authors declare no competing financial interest.

Acknowledgements

This work was supported by the NSF under the CCI Center for Enabling New Technologies through Catalysis (CENTC) Phase II Renewal (CHE-1205189). The authors would like to thank Benjamin Gordon for thoughtful discussions surrounding use of labeling experiments.

References

1. Wang, A.; Li, J.; Zhang, T., Heterogeneous single-atom catalysis. *Nat. Rev. Chem.* **2018**, 2 (6), 65-81.
2. Gates, B. C.; Flytzani-Stephanopoulos, M.; Dixon, D. A.; Katz, A., Atomically dispersed supported metal catalysts: perspectives and suggestions for future research. *Catal. Sci. Technol.* **2017**, 7 (19), 4259-4275.
3. Serna, P.; Gates, B. C., Molecular Metal Catalysts on Supports: Organometallic Chemistry Meets Surface Science. *Acc. Chem. Res.* **2014**, 47 (8), 2612-2620.
4. Copéret, C.; Estes, D. P.; Larmier, K.; Searles, K., Isolated Surface Hydrides: Formation, Structure, and Reactivity. *Chem. Rev.* **2016**, 116 (15), 8463-8505.
5. Hansen, T. W.; DeLaRiva, A. T.; Challa, S. R.; Datye, A. K., Sintering of Catalytic Nanoparticles: Particle Migration or Ostwald Ripening? *Acc. Chem. Res.* **2013**, 46 (8), 1720-1730.
6. Rimoldi, M.; Mezzetti, A., Site isolated complexes of late transition metals grafted on silica: challenges and chances for synthesis and catalysis. *Catal. Sci. Technol.* **2014**, 4 (9), 2724-2740.
7. Coperet, C.; Allouche, F.; Chan, K. W.; Conley, M. P.; Delley, M. F.; Fedorov, A.; Moroz, I. B.; Mougel, V.; Pucino, M.; Searles, K.; Yamamoto, K.; Zhizhko, P. A., Bridging the Gap between Industrial and Well-Defined Supported Catalysts. *Angew. Chem. Int. Ed.* **2018**, 57 (22), 6398-6440.
8. Copéret, C.; Comas-Vives, A.; Conley, M. P.; Estes, D. P.; Fedorov, A.; Mougel, V.; Nagae, H.; Núñez-Zarur, F.; Zhizhko, P. A., Surface Organometallic and Coordination Chemistry toward Single-Site Heterogeneous Catalysts: Strategies, Methods, Structures, and Activities. *Chem. Rev.* **2016**, 116 (2), 323-421.
9. Kim, T.; Celik, F. E.; Hanna, D. G.; Shylesh, S.; Werner, S.; Bell, A. T., Gas-Phase Hydroformylation of Propene over Silica-Supported PPh₃-Modified Rhodium Catalysts. *Top. Catal.* **2011**, 54 (5-7), 299-307.
10. Alt, H. G.; Boehmer, I. K., Catalytic dehydrogenation of isopentane with iridium catalysts. *Angew. Chem. Int. Ed.* **2008**, 47 (14), 2619-2621.
11. Boehmer, I. K.; Alt, H. G., Influence of triphenylphosphine on the activity of heterogeneous iridium, rhodium and platinum containing catalysts for the dehydrogenation of saturated hydrocarbons. *J. Organomet. Chem.* **2009**, 694 (7-8), 1001-1010.
12. Taubmann, S.; Alt, H. G., Heterogeneous catalysts for the dehydrogenation of saturated hydrocarbons. *J. Mol. Catal. A-Chem.* **2008**, 287 (1-2), 102-109.
13. Brünig, J.; Csendes, Z.; Weber, S.; Gorgas, N.; Bittner, R. W.; Limbeck, A.; Bica, K.; Hoffmann, H.; Kirchner, K., Chemoselective Supported Ionic-Liquid-Phase (SILP) Aldehyde Hydrogenation Catalyzed by an Fe(II) PNP Pincer Complex. *ACS Catal.* **2018**, 8 (2), 1048-1051.
14. Annelies, D.; Francis, V.; Bert, S., Opportunities of Immobilized Homogeneous Metathesis Complexes as Prominent Heterogeneous Catalysts. *ChemCatChem* **2016**, 8 (19), 3010-3030.
15. McDonald, A. R.; Dijkstra, H. P., Tethered Pincer Complexes as Recyclable Homogeneous Catalysts. In *The Privileged Pincer-Metal Platform: Coordination Chemistry & Applications*, van Koten, G.; Gossage, R. A., Eds. Springer International Publishing: Cham, 2016; pp 335-369.

16. Neves, A. C. B.; Calvete, M. J. F.; Melo, T.; Pereira, M. M., Immobilized Catalysts for Hydroformylation Reactions: A Versatile Tool for Aldehyde Synthesis. *Eur. J. Org. Chem.* **2012**, (32), 6309-6320.
17. Corma, A.; Garcia, H., Silica-Bound Homogenous Catalysts as Recoverable and Reusable Catalysts in Organic Synthesis. *Adv. Synth. Catal.* **2006**, *348* (12-13), 1391-1412.
18. Riache, N.; Dery, A.; Callens, E.; Poater, A.; Samantaray, M.; Dey, R.; Hong, J.; Li, K.; Cavallo, L.; Basset, J.-M., Silica-Supported Tungsten Carbynes ($\equiv\text{SiO}$)_xW($\equiv\text{CH}$)(Me)_y (x = 1, y = 2; x = 2, y = 1): New Efficient Catalysts for Alkyne Cyclotrimerization. *Organometallics* **2015**, *34* (4), 690-695.
19. Kaphan, D. M.; Klet, R. C.; Perras, F. A.; Pruski, M.; Yang, C.; Kropf, A. J.; Delferro, M., Surface Organometallic Chemistry of Supported Iridium(III) as a Probe for Organotransition Metal-Support Interactions in C-H Activation. *ACS Catalysis* **2018**, *8* (6), 5363-5373.
20. Schöttle, C.; Guan, E.; Okrut, A.; Grosso-Giordano, N. A.; Palermo, A.; Solovyov, A.; Gates, B. C.; Katz, A., Bulky Calixarene Ligands Stabilize Supported Iridium Pair-Site Catalysts. *J. Am. Chem. Soc.* **2019**, *141* (9), 4010-4015.
21. Zhao, Y.; Yang, K. R.; Wang, Z.; Yan, X.; Cao, S.; Ye, Y.; Dong, Q.; Zhang, X.; Thorne, J. E.; Jin, L.; Materna, K. L.; Trimpalis, A.; Bai, H.; Fakra, S. C.; Zhong, X.; Wang, P.; Pan, X.; Guo, J.; Flytzani-Stephanopoulos, M.; Brudvig, G. W.; Batista, V. S.; Wang, D., Stable iridium dinuclear heterogeneous catalysts supported on metal-oxide substrate for solar water oxidation. *Proc. Natl. Acad. Sci. U.S.A.* **2018**, *115* (12), 2902-2907.
22. Zhao, Y.; Yan, X.; Yang, K. R.; Cao, S.; Dong, Q.; Thorne, J. E.; Materna, K. L.; Zhu, S.; Pan, X.; Flytzani-Stephanopoulos, M.; Brudvig, G. W.; Batista, V. S.; Wang, D., End-On Bound Iridium Dinuclear Heterogeneous Catalysts on WO₃ for Solar Water Oxidation. *ACS Cent. Sci.* **2018**, *4* (9), 1166-1172.
23. Kunquan, Y.; William, S.; M., R. J.; Marcus, W.; W., J. C., Evidence that SCS Pincer Pd(II) Complexes are only Precatalysts in Heck Catalysis and the Implications for Catalyst Recovery and Reuse. *Adv. Synth. Catal.* **2005**, *347* (1), 161-171.
24. Moulton, C. J.; Shaw, B. L. Transition Metal-Carbon Bonds. Part XLII. Complexes of Nickel, Palladium, Platinum, Rhodium and Iridium with the Tridentate Ligand 2,6-bis[(di-tert-butylphosphino)methyl]phenyl. *J. Chem. Soc., Dalton Trans.* **1976**, 1020-1024.
25. Kumar, A.; Bhatti, T. M.; Goldman, A. S., Dehydrogenation of Alkanes and Aliphatic Groups by Pincer-Ligated Metal Complexes. *Chem. Rev.* **2017**, *117* (19), 12357-12384.
26. Morales-Morales, D., *Pincer Compounds, Chemistry and Applications*. 1st ed.; Elsevier: 2018.
27. Choi, J.; MacArthur, A. H.; Brookhart, M.; Goldman, A. S., Dehydrogenation and related reactions catalyzed by iridium pincer complexes. *Chem. Rev.* **2011**, *111* (3), 1761-79.
28. Lekich, T. T.; Askelson, P. G.; Burdick, R. K.; Heinekey, D. M., An Improved Synthesis of Me⁴PCP and DMPE. *Organometallics* **2018**, *37* (2), 211-213.
29. Haenel, M. W.; Oevers, S.; Angermund, K.; Kaska, W. C.; Fan, H.-J.; Hall, M. B., Thermally Stable Homogeneous Catalysts for Alkane Dehydrogenation. *Angew. Chem. Int. Ed.* **2001**, *40* (19), 3596-3600.
30. Göttker-Schnetmann, I.; White, P.; Brookhart, M., Iridium Bis(phosphinite) p-XPCP Pincer Complexes: Highly Active Catalysts for the Transfer Dehydrogenation of Alkanes. *J. Am. Chem. Soc.* **2004**, *126* (6), 1804-1811.

31. Göttker-Schnetmann, I.; White, P. S.; Brookhart, M., Synthesis and Properties of Iridium Bis(phosphinite) Pincer Complexes (p-XPCP)IrH₂, (p-XPCP)Ir(CO), (p-XPCP)Ir(H)(aryl), and {(p-XPCP)Ir}₂{μ-N₂} and Their Relevance in Alkane Transfer Dehydrogenation. *Organometallics* **2004**, 23 (8), 1766-1776.
32. Ahuja, R.; Punji, B.; Findlater, M.; Supplee, C.; Schinski, W.; Brookhart, M.; Goldman, A. S., Catalytic dehydroaromatization of n-alkanes by pincer-ligated iridium complexes. *Nat. Chem.* **2010**, 3, 167.
33. Yao, W.; Zhang, Y.; Jia, X.; Huang, Z., Selective Catalytic Transfer Dehydrogenation of Alkanes and Heterocycles by an Iridium Pincer Complex. *Angew. Chem. Int. Ed.* **2014**, 53 (5), 1390-1394.
34. Cohen, S.; Borin, V.; Schapiro, I.; Musa, S.; De-Botton, S.; Belkova, N. V.; Gelman, D., Ir(III)-PC(sp³)P Bifunctional Catalysts for Production of H₂ by Dehydrogenation of Formic Acid: Experimental and Theoretical Study. *ACS Catal.* **2017**, 7 (12), 8139-8146.
35. Bézier, D.; Brookhart, M., Applications of PC(sp³)P Iridium Complexes in Transfer Dehydrogenation of Alkanes. *ACS Catal.* **2014**, 4 (10), 3411-3420.
36. De-Botton, S.; Cohen, S.; Gelman, D., Iridium PC(sp³)P Pincer Complexes with Hemilabile Pendant Arms: Synthesis, Characterization, and Catalytic Activity. *Organometallics* **2018**, 37 (8), 1324-1330.
37. Polukeev, A. V.; Wendt, O. F., Cyclohexane-Based Phosphinite Iridium Pincer Complexes: Synthesis, Characterization, Carbene Formation, and Catalytic Activity in Dehydrogenation Reactions. *Organometallics* **2017**, 36 (3), 639-649.
38. Hermann, D.; Gandelman, M.; Rozenberg, H.; Shimon, L. J. W.; Milstein, D., Synthesis, Structure, and Reactivity of New Rhodium and Iridium Complexes, Bearing a Highly Electron-Donating PNP System. Iridium-Mediated Vinylic C–H Bond Activation. *Organometallics* **2002**, 21 (5), 812-818.
39. Ito, J.-i.; Shiomi, T.; Nishiyama, H., Efficient Preparation of New Rhodium- and Iridium-[Bis(oxazolonyl)-3,5-dimethylphenyl] Complexes by C-H Bond Activation: Applications in Asymmetric Synthesis. *Adv. Synth. Catal.* **2006**, 348 (10-11), 1235-1240.
40. Allen, K. E.; Heinekey, D. M.; Goldman, A. S.; Goldberg, K. I., Alkane Dehydrogenation by C–H Activation at Iridium(III). *Organometallics* **2013**, 32 (6), 1579-1582.
41. Paredes, P.; Díez, J.; Gamasa, M. P., Synthesis of Enantiopure Iridium(I) and Iridium(III) Pybox Complexes and Their Application in the Asymmetric Transfer Hydrogenation of Ketones. *Organometallics* **2008**, 27 (11), 2597-2607.
42. Miller, A. J. M., Controlling ligand binding for tunable and switchable catalysis: cation-modulated hemilability in pincer-crown ether ligands. *Dalton Trans.* **2017**, 46 (36), 11987-12000.
43. Kumar, A.; Zhou, T.; Emge, T. J.; Mironov, O.; Saxton, R. J.; Krogh-Jespersen, K.; Goldman, A. S., Dehydrogenation of n-Alkanes by Solid-Phase Molecular Pincer-Iridium Catalysts. High Yields of alpha-Olefin Product. *J. Am. Chem. Soc.* **2015**, 137 (31), 9894-911.
44. Rimoldi, M.; Fodor, D.; van Bokhoven, J. A.; Mezzetti, A., A stable 16-electron iridium(III) hydride complex grafted on SBA-15: a single-site catalyst for alkene hydrogenation. *Chem. Commun. (Camb)* **2013**, 49 (96), 11314-6.
45. Rimoldi, M.; Fodor, D.; van Bokhoven, J. A.; Mezzetti, A., Catalytic hydrogenation of liquid alkenes with a silica-grafted hydride pincer iridium(III) complex: support for a heterogeneous mechanism. *Catal. Sci. Technol.* **2015**, 5 (9), 4575-4586.

46. Rimoldi, M.; Mezzetti, A., Silica-Grafted 16-Electron Hydride Pincer Complexes of Iridium(III) and Their Soluble Analogues: Synthesis and Reactivity with CO. *Inorg. Chem.* **2014**, *53* (22), 11974-11984.
47. Rimoldi, M.; Mezzetti, A., Batch and Continuous Flow Hydrogenation of Liquid and Gaseous Alkenes Catalyzed by a Silica-grafted Iridium(III) Hydride. *Helv. Chim. Acta* **2016**, *99* (12), 908-915.
48. Rimoldi, M.; Nakamura, A.; Vermeulen, N. A.; Henkelis, J. J.; Blackburn, A. K.; Hupp, J. T.; Stoddart, J. F.; Farha, O. K., A metal-organic framework immobilised iridium pincer complex. *Chem. Sci.* **2016**, *7* (8), 4980-4984.
49. Chanthateyanonth, R.; Alper, H., The first synthesis of stable palladium(II) PCP-type catalysts supported on silica—application to the Heck reaction. *J. Mol. Catal. A-Chem.* **2003**, *201* (1), 23-31.
50. Ratana, C.; Howard, A., Recyclable Tridentate Stable Palladium(II) PCP-Type Catalysts Supported on Silica for the Selective Synthesis of Lactones. *Adv. Synth. Catal.* **2004**, *346* (11), 1375-1384.
51. Giménez, R.; Swager, T. M., Dinuclear pincer-palladium(II) complexes and their use as homogeneous or heterogeneous catalyst for the aldol reaction of methyl isocyanoacetate. *J. Mol. Catal. A-Chem.* **2001**, *166* (2), 265-273.
52. Sommer, W. J.; Yu, K.; Sears, J. S.; Ji, Y.; Zheng, X.; Davis, R. J.; Sherrill, C. D.; Jones, C. W.; Weck, M., Investigations into the Stability of Tethered Palladium(II) Pincer Complexes during Heck Catalysis. *Organometallics* **2005**, *24* (18), 4351-4361.
53. Mehendale, N. C.; Bezemer, C.; van Walree, C. A.; Klein Gebbink, R. J. M.; van Koten, G., Novel silica immobilized NCN-pincer palladium(II) and platinum(II) complexes: Application as Lewis acid catalysts. *J. Mol. Catal. A-Chem.* **2006**, *257* (1), 167-175.
54. C., M. N.; A., S. J. R.; P., d. J. K.; A., v. W. C.; Klein, G. R. J. M.; Gerard, v. K., PCP- and SCS-Pincer Palladium Complexes Immobilized on Mesoporous Silica: Application in C-C Bond Formation Reactions. *Adv. Synth. Catal.* **2007**, *349* (17-18), 2619-2630.
55. Goni, M. A.; Rosenberg, E.; Gobetto, R.; Chierotti, M., Dehydrogenative coupling of alcohols to esters on a silica polyamine composite by immobilized PNN and PONOP pincer complexes of ruthenium. *J. Organomet. Chem.* **2017**, *845*, 213-228.
56. Goni, M. A.; Rosenberg, E.; Meregude, S.; Abbott, G., A methods study of immobilization of PONOP pincer transition metal complexes on silica polyamine composites (SPC). *J. Organomet. Chem.* **2016**, *807*, 1-10.
57. Huang, Z.; Brookhart, M.; Goldman, A. S.; Kundu, S.; Ray, A.; Scott, S. L.; Vicente, B. C., Highly Active and Recyclable Heterogeneous Iridium Pincer Catalysts for Transfer Dehydrogenation of Alkanes. *Adv. Synth. Catal.* **2009**, *351* (1-2), 188-206.
58. Huang, Z.; Rolfe, E.; Carson, E. C.; Brookhart, M.; Goldman, A. S.; El-Khalafy, S. H.; MacArthur, A. H. R., Efficient Heterogeneous Dual Catalyst Systems for Alkane Metathesis. *Adv. Synth. Catal.* **2010**, *352* (1), 125-135.
59. Vicente, B. C.; Huang, Z.; Brookhart, M.; Goldman, A. S.; Scott, S. L., Reactions of phosphinites with oxide surfaces: a new method for anchoring organic and organometallic complexes. *Dalton Trans.* **2011**, *40* (16), 4268-74.
60. Sheludko, B.; Cunningham, M. T.; Goldman, A. S.; Celik, F. E., Continuous-Flow Alkane Dehydrogenation by Supported Pincer-Ligated Iridium Catalysts at Elevated Temperatures. *ACS Catal.* **2018**, *8* (9), 7828-7841.

61. Kubelka, P., New Contributions to the Optics of Intensely Light-Scattering Materials. Part II: Nonhomogeneous Layers*. *J. Opt. Soc. Am.* **1954**, *44* (4), 330-335.
62. Kubelka, P. M., F., Ein Beitrag zur Optik der Farbanstriche. *Z. Techn. Physik.* **1931**, *12*, 593-601.
63. Wojdyr, M., *J. Appl. Cryst.* **2010**, *43*, 1126-1128.
64. Tooke, P. B., Fourier self-deconvolution in IR spectroscopy. *TrAC – Trend. Anal. Chem.* **1988**, *7* (4), 130-136.
65. OriginPro 2019, A. V. O. C., Northampton, MA, USA.
66. Marquardt, D. W., An Algorithm for Least-Squares Estimation of Nonlinear Parameters. *J. Soc. Ind. Appl. Math.* **1963**, *11* (2), 431-441.
67. Levenberg, K., A method for the solution of certain non-linear problems in least squares. *Quart. Appl. Math.* **1944**, *2*.
68. Vicente, B. C.; Huang, Z.; Brookhart, M.; Goldman, A. S.; Scott, S. L., Reactions of phosphinites with oxide surfaces: a new method for anchoring organic and organometallic complexes. *Dalton Trans.* **2011**, *40* (16), 4268-4274.
69. Romero, P. E.; Whited, M. T.; Grubbs, R. H., Multiple C–H Activations of Methyl tert-Butyl Ether at Pincer Iridium Complexes: Synthesis and Thermolysis of Ir(I) Fischer Carbenes1. *Organometallics* **2008**, *27* (14), 3422-3429.
70. Zhao, Y.; Yang, K. R.; Wang, Z.; Yan, X.; Cao, S.; Ye, Y.; Dong, Q.; Zhang, X.; Thorne, J. E.; Jin, L.; Materna, K. L.; Trimpalis, A.; Bai, H.; Fakra, S. C.; Zhong, X.; Wang, P.; Pan, X.; Guo, J.; Flytzani-Stephanopoulos, M.; Brudvig, G. W.; Batista, V. S.; Wang, D., Stable iridium dinuclear heterogeneous catalysts supported on metal-oxide substrate for solar water oxidation. *Proc. Natl. Acad. Sci. U.S.A.* **2018**, *115* (12), 2902-2907.
71. Goldberg, J. M.; Cherry, S. D. T.; Guard, L. M.; Kaminsky, W.; Goldberg, K. I.; Heinekey, D. M., Hydrogen Addition to (pincer)IrI(CO) Complexes: The Importance of Steric and Electronic Factors. *Organometallics* **2016**, *35* (20), 3546-3556.
72. Goldberg, J. M.; Wong, G. W.; Brastow, K. E.; Kaminsky, W.; Goldberg, K. I.; Heinekey, D. M., The Importance of Steric Factors in Iridium Pincer Complexes. *Organometallics* **2015**, *34* (4), 753-762.
73. Jonasson, K. J.; Polukeev, A. V.; Wendt, O. F., PC(sp³)P pincer carbonyl complexes of iridium(I), and iridium(III). *RSC Adv.* **2015**, *5* (20), 15534-15538.
74. Gregor, L. C.; Grajeda, J.; White, P. S.; Vetter, A. J.; Miller, A. J. M., Salt-promoted catalytic methanol carbonylation using iridium pincer-crown ether complexes. *Catal. Sci. Technol.* **2018**, *8* (12), 3133-3143.
75. Grajeda, J.; Kita, M. R.; Gregor, L. C.; White, P. S.; Miller, A. J. M., Diverse Cation-Promoted Reactivity of Iridium Carbonyl Pincer-Crown Ether Complexes. *Organometallics* **2016**, *35* (3), 306-316.
76. Zhuravlev, L. T., Concentration of hydroxyl groups on the surface of amorphous silicas. *Langmuir* **1987**, *3* (3), 316-318.

For Table of Contents Only

